Turbulent channel flow controlled by traveling wave-like body force mimicking oscillating thin films

R. Yamamoto (山本 遼),[1] J. Morita (森田 淳一),[1] H. Mamori (守 裕也)*,[1] T. Miyazaki (宮嵜 武),[1] and S. Hara (原 峻平)[2]

[1)]*Department of Mechanical and Intelligent Systems Engineering, The University of Electro-Communications, 1-5-1, Chofugaoka, Chofu, Tokyo 182-8585, Japan,*

*(*Electronic mail: corresponding author, mamori@uec.ac.jp)*

[2)]*Department of Mechanical Engineering, Doshisha University, 1-3 Tatara Miyakodani, Kyotanabe-shi, Kyoto 610-0394, Japan*

(Dated: 30 June 2022)

To improve energy efficiency, flow control techniques for skin-friction drag and heat transfer with regard to wall turbulence are essential. This study performs direct numerical simulation of turbulent channel flows. The traveling-wave-like body force is employed as the flow control technique to break the similarity between momentum and heat transfer. The traveling wave control mimics the self-excited thin film in the corresponding experimental study. When the wave traveled slowly along the downstream direction, the skin-friction drag, heat transfer, and analogy factor are found to increase. Moreover, these parameters increased with an increase in the reference height of the traveling wave (h_w). Flow visualization shows turbulence enhancement owing to the increase in h_w. Three-component decomposition elucidates the difference between the control effect on the Reynolds shear stress and the turbulent heat flux.

I. INTRODUCTION

As energy consumption increases annually with population growth, efficient energy utilization is essential to achieve energy saving and reduce environmental impact. "Make energy clean for all" is one of the primary sustainable development goals (SDGs). In fluid engineering, the development of flow control techniques to reduce energy loss is receiving considerable attention. As skin-friction drag significantly increases in turbulent wall flows, the control of turbulent flow is essential. This is expected to contribute to industrial, economic, and other issues. In particular, a flow control technique to enhance heat transfer and reduce skin-friction drag is a challenging issue because there is a substantial similarity between the momentum and heat transports, known as the Reynolds or Colburn analogy. The analogy in the governing equations of momentum and energy is confirmed and the definition of skin friction and heat transfer is examined. In addition, the identity equations for the skin-friction coefficient and Nusselt number are identical[1,2], in which the turbulent contribution is obtained by integrating the Reynolds shear stress (RSS) and turbulent heat flux (THF). Accordingly, the analogy holds, and achieving flow control such that the analogy breaks is difficult. If flow control techniques decrease the turbulence or suppress the activity of vortical structures, the skin-friction drag and heat transfer decrease. Conversely, if the flow control techniques promote turbulence, the drag and heat transfer increase.

To break the similarity between the momentum and heat transfer, Hasegawa and Kasagi[3] derived a control law based on the suboptimal control theory for feedback control using blowing and suction from the wall in a fully developed turbulent channel flow. They demonstrated that the control exhibited a dissimilar effect. Specifically, the tripled heat transfer and skin-friction drag were doubled compared with the uncontrolled case. Yamamoto *et al.*[4] derived a control law based on the optimal control theory and observed a 30% decrease in the skin friction drag and a doubling in the heat transfer. In addition to feedback control, predetermined control has been investigated in relation to the dissimilarity effect. The traveling-wave control is one of the predetermined control to decrease the skin-friction drag in the wall turbulence (e.g., Mamori *et al.*[5]; Koganezawa *et al.*[6]; Nabae and Fukagata[7,8]). Uchino et al.[9] employed traveling-wave-like wall deformation control[10–12] for a fully developed turbulent channel flow and reported a heat transfer enhancement of up to 13%. According to Hasegawa and Kasagi[3], the resultant blowing and suction distribution yielded traveling-wave-like control. Based on these studies, Kaithakkal *et al.*[13] employed traveling-wave-like blowing and suction to generate a dissimilarity effect. Ogino *et al.*[14]

and Mamori *et al.*[15] investigated the drag reduction and heat transfer effects based on the traveling wave in the Taylor–Couette flow, respectively. Accordingly, the traveling wave propagating on the wall surface can induce a dissimilar effect between the momentum and heat transport. Murakami and Hara[16] recently conducted an experimental study to investigate the effect of the self-excited oscillation of thin films in turbulent channel flow, and they revealed that the wave affects skin-friction drag and heat transfer. The film was installed in the flow passage, and wave propagation directly affected the flow.

Inspired by Murakami and Hara[16], direct numerical simulation (DNS) of turbulent channel flow is performed to investigate the effect of the dissimilarity between the transports based on the wave propagating in the flow. Since the dissimilarity is known to be related to the vortical structure of the turbulence in accordance with the previous study, the DNS is suited for the objective of resolving it. To mimic the self-excited oscillation of a thin film, a traveling-wave-like body force[5,17] is employed. Although the control effect due to the body force would be different from that of the thin film (e.g., the body force allows penetration of the flow along the wall-normal direction), the direct control effect of the turbulent flow using the ideal body force is expected.

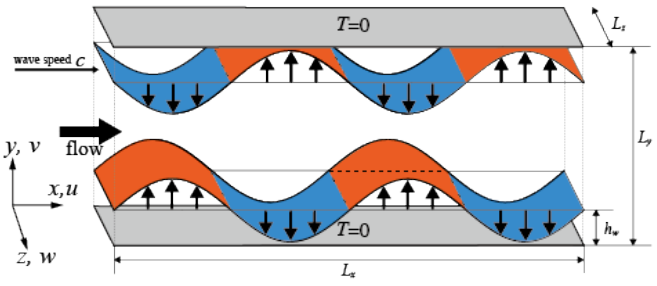

FIG. 1. Schematic and parameters of the traveling wave.

II. DIRECT NUMERICAL SIMULATION

DNSs of the fully developed channel-flow turbulence controlled by the body force in the form of traveling waves is performed. Figure 1 shows the schematic of the channel flow, and the computational domain is $L_x \times L_y \times L_z = 2\pi \times 2 \times \pi$. The governing equations are the continuity, Navier–Stokes, and energy equations, which are expressed as

$$\frac{\partial u_i}{\partial x_i} = 0, \tag{1}$$

$$\frac{\partial u_i}{\partial t} + \frac{\partial u_j u_i}{\partial x_j} = -\frac{\partial P}{\partial x_i} - \frac{\partial p}{\partial x_i} + \frac{1}{\mathrm{Re}_\tau}\frac{\partial^2 u_i}{\partial x_j \partial x_j} + F_i, \tag{2}$$

$$\frac{\partial T}{\partial t} + \frac{\partial u_j T}{\partial x_j} = Q + \frac{1}{\mathrm{Re}_\tau \mathrm{Pr}}\frac{\partial^2 T}{\partial x_j \partial x_j}, \tag{3}$$

where t and P are time and pressure, respectively. x, y, and z are the coordinate system components; u, v, and w are the velocities along the corresponding directions; T is the temperature; F is the body force (or the control input); Q is the heat source term. The temperature is treated as a passive scalar. All variables are nondimensionalized by the friction velocity u_τ^* and channel half-width δ^*, where the asterisk indicates dimensional variables. The friction Reynolds number and Prandtl number are defined as follows:

$$\mathrm{Re}_\tau = \frac{u_\tau^* \delta^*}{\nu^*}, \quad \mathrm{Pr} = \frac{\nu^*}{\alpha^*}, \tag{4}$$

where the kinematic viscosity is ν^* and the thermal diffusivity is α^*. To maintain the similarity between momentum and heat transport, the constant pressure gradient (i.e., $-dP/dx = 1$) and uniform heat generation conditions are imposed ($Q = 1$), and the Prandtl number is set to $\mathrm{Pr} = 1$. The friction Reynolds number is set to $\mathrm{Re}_\tau = 180$, corresponding to the bulk Reynolds number of 5600. The periodic boundary condition is imposed along the homogenous direction, and the

velocity and temperature are zero on the wall. The simulations initiate from the fully developed turbulent channel flow at $\mathrm{Re}_\tau = 180$.

In the DNS code (in-house code), an energy conservative second-order central difference method[18,19] is employed to discretize the governing equations in space; for the time integration, the second-order Crank-Nicolson and third-order Runge-Kutta schemes are used for the viscosity and convection terms, respectively; the simplified marker and cell method are used for the velocity and pressure coupling. The computational resources and time are added in the following. The present DNS employs the direct method with the FFT for coupling the velocity and the pressure. Therefore, the iteration method is not employed, and the residual of the continuity equation is machine zero at all the time steps. The employed CPU is intel Xeon Silver 4216 (16Core-2.1GHz) and parallel computing is made by 32 threads with 2 CPUs. The total CPU time for each calculation to obtain the statistics was 27 hours at the least. For single computation, the time step is 5×10^{-4} and the total integration time is 100.

The control input is a traveling-wave-like wall-normal body force, which is expected to induce wall-normal velocity to mimic the control effect of self-excited thin films[16]. For the lower half of the channel, the body force term is imposed as

$$F_x = F_z = 0, \tag{5}$$

$$F_y = A \exp\left(-\frac{|y - h_w|}{\Delta}\right) \cos\left(\frac{2\pi}{\lambda}(x - ct)\right), \tag{6}$$

The wave travels along the streamwise direction and is uniform along the spanwise direction. The control parameters are the amplitude of the wave A, reference position h_w, influence height Δ, wavelength λ, and wave speed c. To mimic the deformation of the thin film, the body force activates at $(y - h_w) < \Delta$ for the first half of the wavelength and $-(y - h_w) < \Delta$ for the second half. In this study, the amplitude is fixed at $A = 500$[5,17], and the downstream traveling wave $c > 0$ is investigated. The symmetry of body force distribution is imposed on the upper half of the channel.

TABLE I. Number of grid points and domain

	$N_x \times N_y \times N_z$	$L_x \times L_y \times L_z$
Super coarse grid	$128 \times 96 \times 128$	$2\pi \times 2 \times \pi$
Coarse grid	$256 \times 192 \times 256$	$2\pi \times 2 \times \pi$
Fine grid	$256 \times 384 \times 128$	$2\pi \times 2 \times \pi$
Super fine grid	$512 \times 768 \times 256$	$2\pi \times 2 \times \pi$
Lage Domain	$512 \times 394 \times 256$	$4\pi \times 2 \times \pi$

To validate the grid resolution and computational domain size, the results of the uncontrolled and controlled flows are compared in different runs (Table I). Figure 2 shows the RMS values of the velocity of the uncontrolled flow with the existing DNS data[20]. The results indicate that the difference between the statistics in each domain is small. In addition, Fig. 3 shows the RMS values of the controlled flow for $A = 500$, $\Delta = 0.1$, $h_w = 0.5$, $\lambda = \pi$, and $c = 10$. A reasonable agreement among the statistics has been confirmed. Accordingly, a fine grid is employed to investigate the control effect in detail. The fine grid exhibits uniform grid spacing along the homogeneous wall-normal directions because the traveling wave control is applied to the flow and the grid resolution is required in the entire domain.

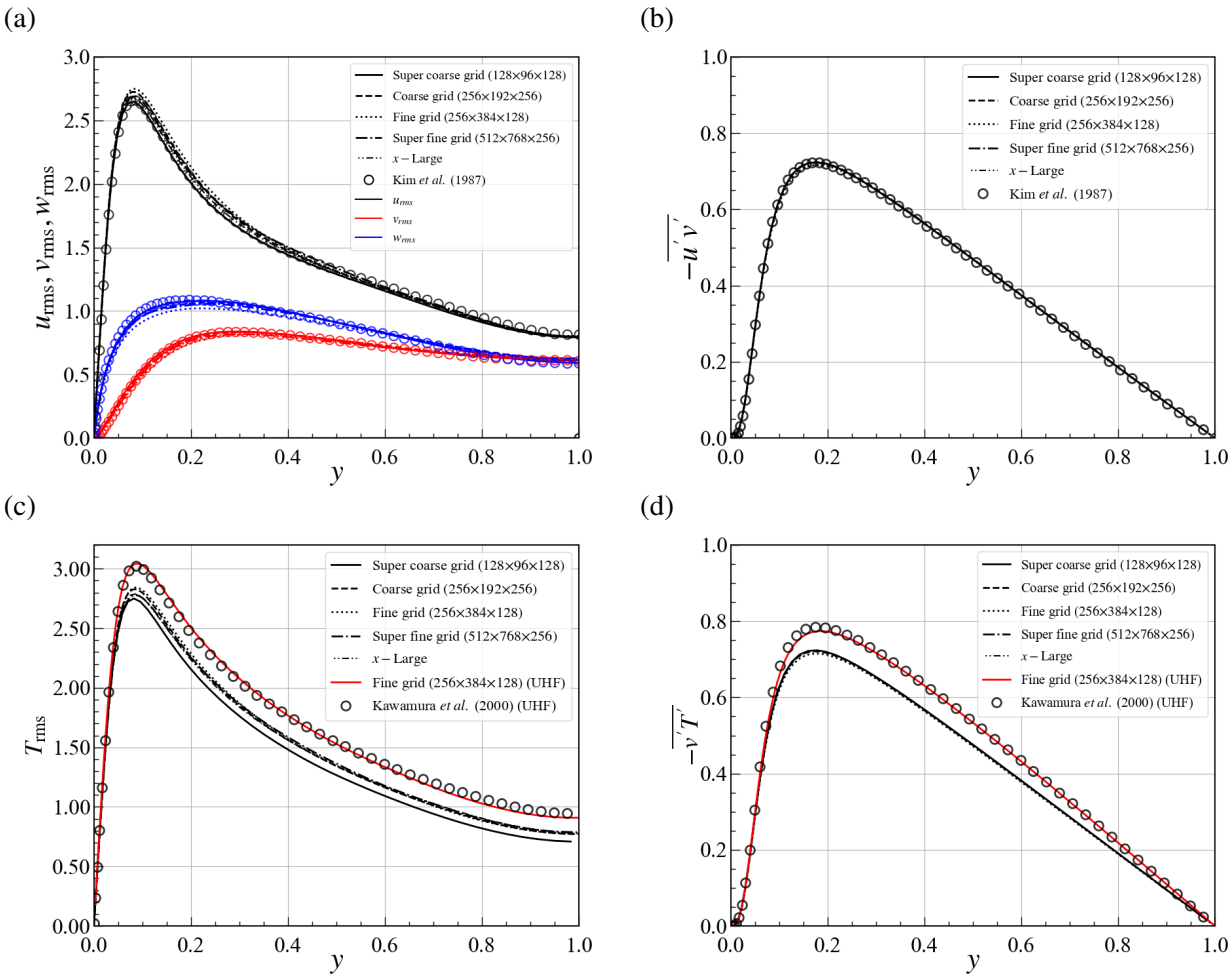

FIG. 2. Flow statistics of the uncontrolled flow for different runs: (a) the rms value of velocities, (b) the Reynolds shear stress, (c) the rms value of temperature, and (d) the turbulent heat flux. Solid line, super coarse grid; broken line, coarse grid; dotted line, fine grid; single-dot chain line, super fine grid; two-dot chain line, large domain; red line, fine grid and the uniform heat flux condition (referred as the UHF); circle, Kim *et al.*[20] or Kawamura *et al.*[21]. Black, red, and blue curves represent u_{rms}, v_{rms}, and w_{rms}, respectively.

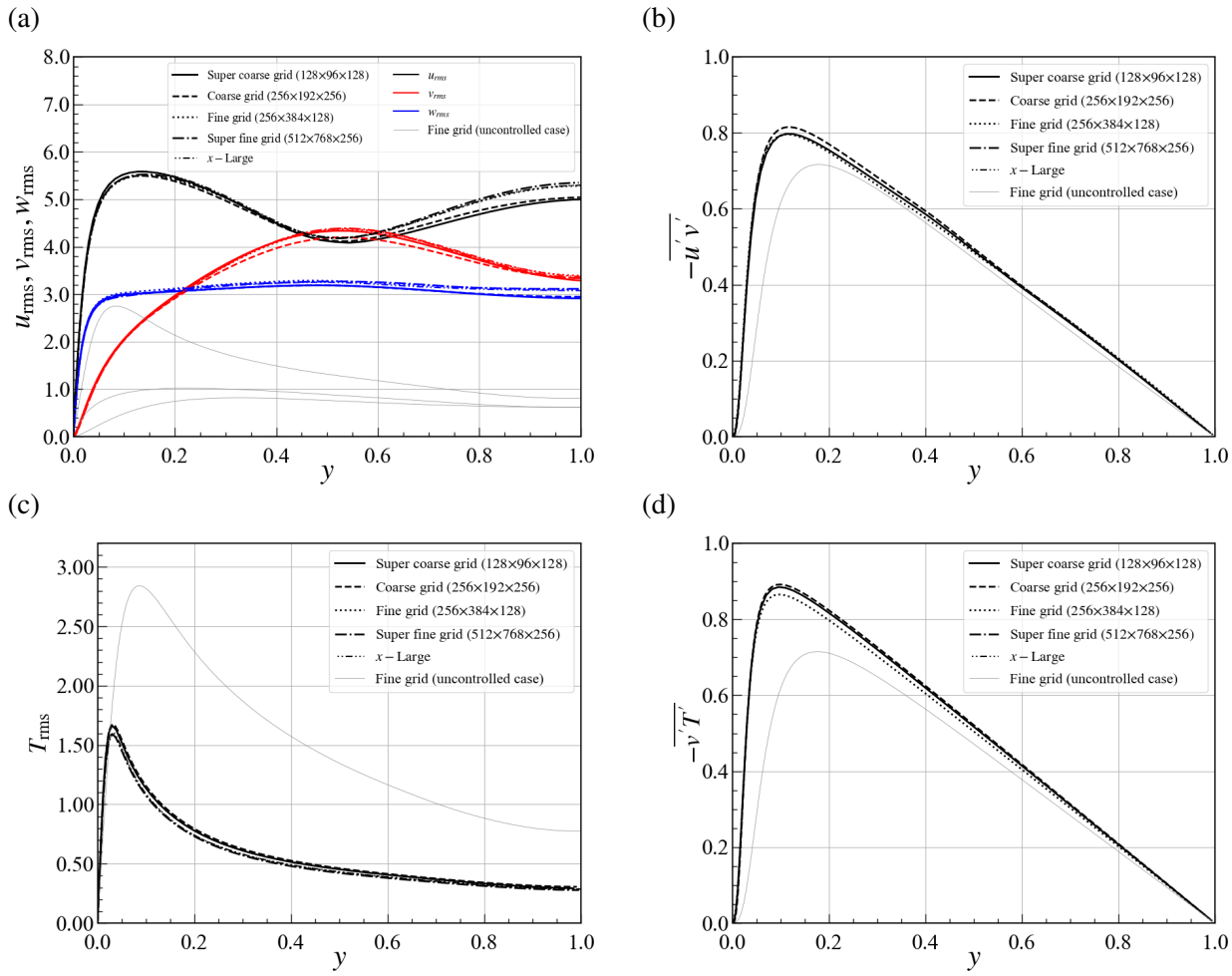

FIG. 3. Flow statistics of the controlled flow for different runs: (a) the rms value of velocities, (b) the Reynolds shear stress, (c) the rms value of temperature, and (d) the turbulent heat flux. Sold line, super coarse grid; broken line, coarse grid; dotted line, fine grid; single-dot chain line, super fine grid; two-dot chain line, large domain; thin line, fine grid and the uncontrolled flow. The details of computational conditions are shown in Table I. Black, red, and blue curves represent u_{rms}, v_{rms}, and w_{rms}, respectively. The control parameters are $A = 500$, $\Delta = 0.1$, $h_w = 0.5$, $\lambda = \pi$, and $c = 10$.

TABLE II. Comparison of the control performances by the traveling wave-like blowing and suction case at $a = 0.035$, $\lambda = 1.12$, and $c = 0.15$.

	$L_x \times L_y \times L_z$	$N_x \times N_y \times N_z$	Re_b	Re_τ	C_f/C_{f0}	$\mathrm{St}/\mathrm{St}_0$	$(2\mathrm{St}/C_f)/(2\mathrm{St}_0/C_{f0})$
Present DNS	$6.72 \times 2 \times \pi$	$256 \times 384 \times 128$	4586	148	1.28	2.12	1.65
Kaithakkal *et al.*[13]	$5\pi \times 2 \times \pi$	$128 \times 65 \times 128$	4586	150	1.26	2.12	1.69

For the validation of the DNS code, the DNS of the channel flow is controlled by the traveling wave-like blowing, and suction is made. The control input is the wall-normal velocity from the wall as

$$v_{w\pm} = \mp a \cos\left(\frac{2\pi}{\lambda}(x - ct)\right) \tag{7}$$

where a is the amplitude of the wave, and v_{w+} and v_{w-} are the wall-normal velocity from the upper and lower walls. The other velocity components and the temperature are zero on the wall. Unlike the main DNS, the constant flow rate condition is imposed, and the body force is zero (i.e., $F_i = 0$). The heat source term is imposed to be the same as the mean pressure gradient (i.e., $Q = -\partial P/\partial z$). The results are compared with the numerical simulation by Kaithakkal *et al.*[13]: they employed the pseudo-spectral method with Fourier expansion in the homogeneous directions and Chebyshev polynomials in the wall-normal direction for spatial discretization. The control parameters are $a = 0.035$, $\lambda = 1.12$, $c = 0.15$. Note that the reference length and the velocity are δ^* and twice the bulk mean velocity ($2u_b^*$). The numerical conditions and the results are shown in Table II.

The subscript of zero means the uncontrolled flow, and C_f and St are the skin-friction coefficient, and the Stanton number, respectively. The definition of C_f is shown in the next section, and the Stanton number is defined as

$$\mathrm{St} = \frac{q_w^*}{\rho^* C_p^* u_b^* T_b^*}, \tag{8}$$

where q_w^*, C_p^*, and T_b^* are the heat flux at the wall, the heat capacity of the fluid, and the bulk mean temperature, respectively. While the present DNS overestimates the skin-friction coefficient and underestimates the analogy factor slightly, the discrepancy is reasonably accepted. Therefore, the present DNS well reproduces the results by Kaithakkal *et al.*[13]

III. RESULTS AND DISCUSSIONS

The performance of the control is investigated. The skin-friction coefficient C_f and Nusselt number Nu are considered as the cost functions, as follows.

$$C_f = \frac{\tau_w^*}{\frac{1}{2}\rho^* u_b^*} = \frac{4}{\mathrm{Re}_b}\frac{1}{u_b}\left(\left.\frac{\partial \bar{u}}{\partial n}\right|_{\mathrm{wall}}\right), \quad \mathrm{Nu} = \frac{2\delta^* h^*}{k^*} = \frac{2}{T_b}\left(-\left.\frac{\partial T}{\partial n}\right|_{\mathrm{wall}}\right), \tag{9}$$

where τ_w^* denotes the wall friction, u_b^* denotes the bulk mean velocity, ρ^* denotes the fluid density, h^* denotes the heat transfer, and k^* denotes the thermal conductivity. The bulk mean velocity u_b and temperature T_b are defined as

$$u_b = \frac{1}{2}\int_0^2 \bar{u} dy, \quad T_b = \frac{1}{2u_b}\int_0^2 \overline{uT} dy, \tag{10}$$

where the bar denotes the temporal and spatial average in the homogeneous directions. The j/f factor indicates the dissimilarity between the momentum and heat transfer and is defined as

$$j/f = \frac{\mathrm{Nu}}{\mathrm{Pr}^{1/3}\mathrm{Re}_b}\frac{1}{4C_f}, \tag{11}$$

where Re_b denotes the Reynolds number based on the bulk velocity u_b.

The dependency of the control parameter on the control performance is demonstrated. Here, the range of the control parameter is based on Mamori and Fukagata[5], who investigated the drag reduction effect based on the traveling-wave-like body force from the wall (i.e., $h_w = 0$). Figure 4 shows the dependency of the time-averaged C_f, Nu, and j/f factor as a function of c or h_w. These values are normalized by those of the uncontrolled flow of $\mathrm{Re}_\tau = 180$, denoted by zero subscripts. Figure 4(a) shows the dependency of c, and the other parameters are fixed at $h_w = 0.5$, $\Delta = 0.1$, $A = 500$, and $\lambda = \pi$. The skin-friction coefficient and Nusselt number peak at $c = 10$, and they decrease as the wave speed increases. Moreover, the j/f factor peaks at $c = 10$, indicating that the dissimilarity between momentum and heat is strengthened. This trend is similar to the case of traveling-wave-like blowing and suction on the wall surface[13], and the maximum analogy factor was obtained by the downstream traveling wave with a wave speed of 30% of the mean bulk velocity. Figure 4(b) shows the dependency of h_w on $\Delta = 0.1$, $A = 500$, $c = 11$, and $\lambda = \pi$. The Nusselt number and skin-friction coefficient increase with an increase in h_w, whereas they slightly decrease at large values of h_w. Moreover, the j/f factor increases, and the maximum value is obtained at $h_w = 0.6$. There are explained by the twofold reasons. First, the wave promotes the turbulence (i.e., corresponding to the increase of the random component), which relates to the

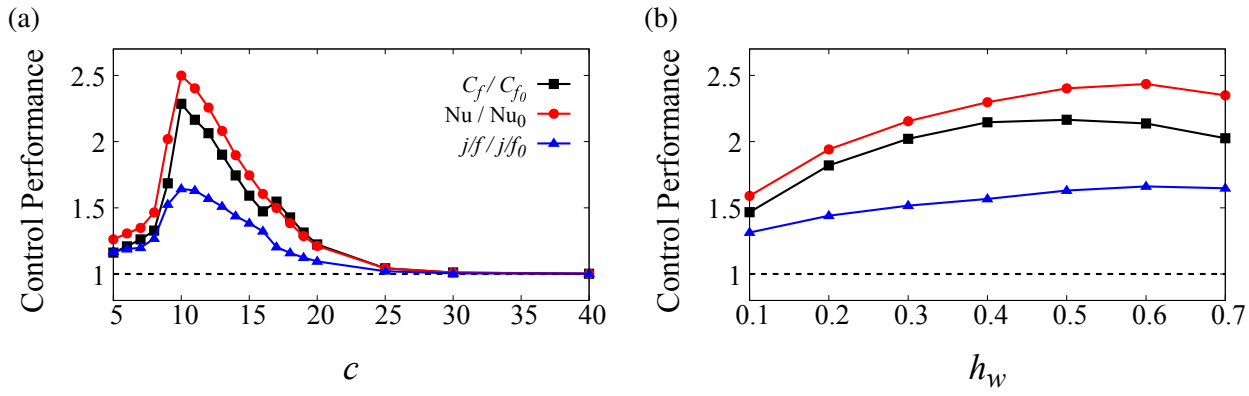

FIG. 4. Dependency of (a) c ($h_w = 0.5$, $\Delta = 0.1$, $A = 500$, and $\lambda = \pi$) and (b) h_w ($\Delta = 0.1$, $A = 500$, $c = 11$, and $\lambda = \pi$) on the skin-friction coefficient, Stanton number, and j/f factor. They are normalized to those of the uncontrolled values.

production of the turbulence in the buffer layer. Second, the wave creates the Reynolds shear stress and the turbulent heat flux as the coherent component. If h_w is small, they are created in the near wall region, and the contribution to the skin-friction drag and the heat flux is significant. However, if h_w is large, they are created away from the wall, and the contribution decrease[1,2].

The range of the high control performance is comparable with the mean bulk velocity of the uncontrolled flow, which is in accordance with the results of the traveling-wave-like blowing/suction[13,22] and wall deformation[9] cases. However, turbulent mixing enhances when h_W increases. The following cases are chosen to discuss the effect of h_w on the flow field: Case NC, the uncontrolled case; Case 1, $h_w = 0.1$; Case 2, $h_w = 0.5$; Case 3, $h_w = 0.7$. For the controlled cases (Cases 1$\sim$3), other control parameters are fixed at $\Delta = 0.1$, $A = 500$, $c = 11$, and $\lambda = \pi$.

Figure 5 shows the instantaneous flow fields of u and w on the $x-y$ plane. The spanwise velocity in the region near the wall corresponds to the turbulent vortical structures in the region near the wall. Therefore, in Case 1, the contraction and expansion of the velocity vector are observed, which corresponds to the flow acceleration and deceleration, respectively. The traveling wave creates a spanwise vortex, which affects the base flow[5]. As h_w increases, the contraction strengthens in Case 2, whereas it is not clearly observed in Case 3. The spanwise velocity fluctuates in Cases 2 and 3, which implies the promotion of turbulence compared with Case NC.

Figure 6 shows the instantaneous vortical structure and streamwise velocity on the $x-y$ plane for each case. The vortical structures are visualized by the second invariant of the velocity deformation tensor (i.e., the Q value). The threshold values of the vortical structures are $Q^+ = 0.03$ for Case NC and $Q^+ = 0.17$ for other cases, where the superscript plus denotes the wall unit based on

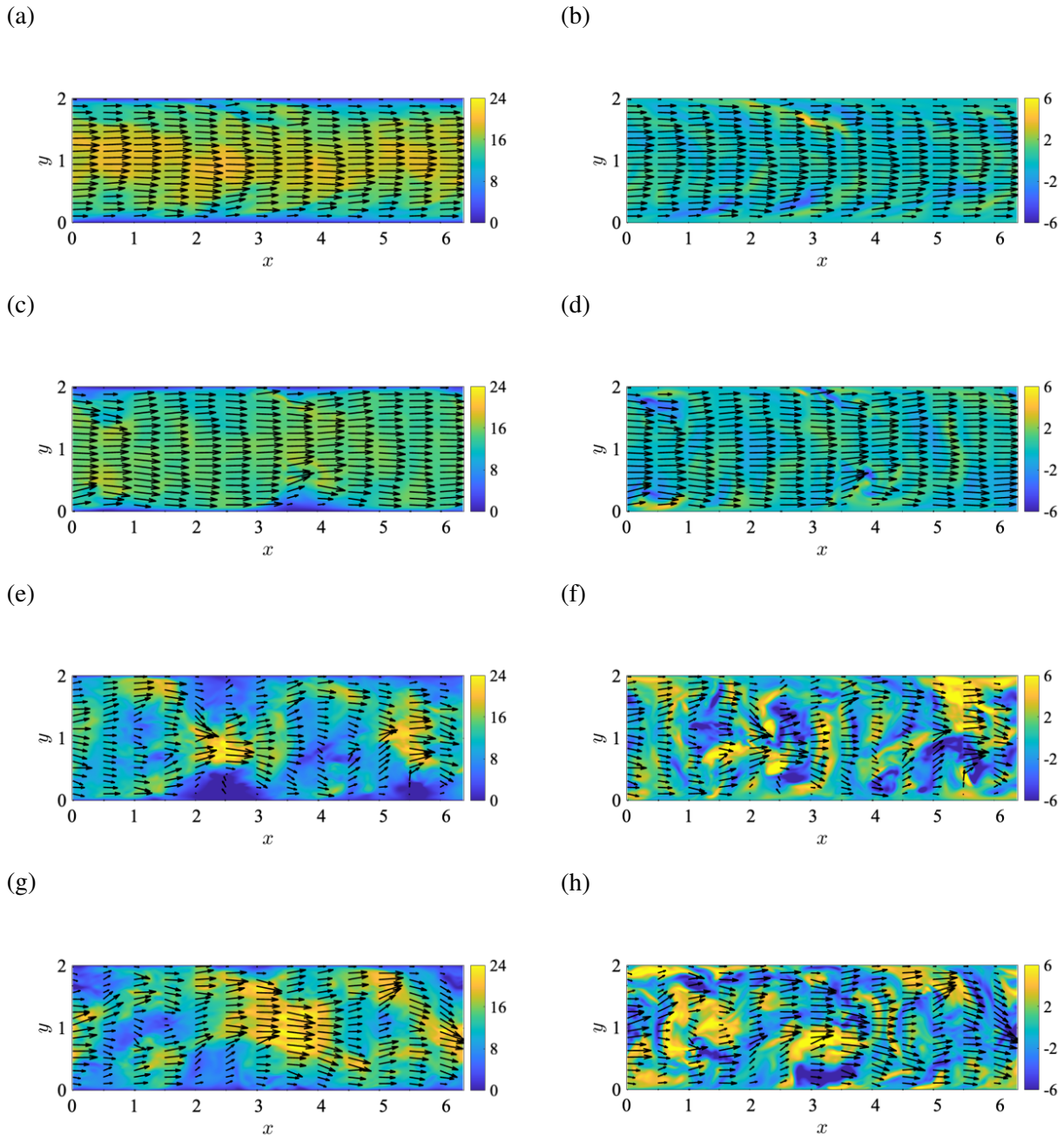

FIG. 5. Instantaneous flow field with the velocity vector on the x-y plane at $z = 0$: (a,b) Case NC, (c,d) Case 1, (e,f) Case 2, and (g,h) Case 3. The left and right columns represent the streamwise and spanwise velocities, respectively.

the friction velocity of Case NC. Different threshold values are used because the skin friction drag in the controlled cases is significantly larger than that in Case NC. In Case NC, vortical structures are observed in the region near the wall. In Case 1, vortical structures are observed, which corresponds to the contraction region (Fig. 5(c-d)). When h_w increases in Cases 2 and 3, the number

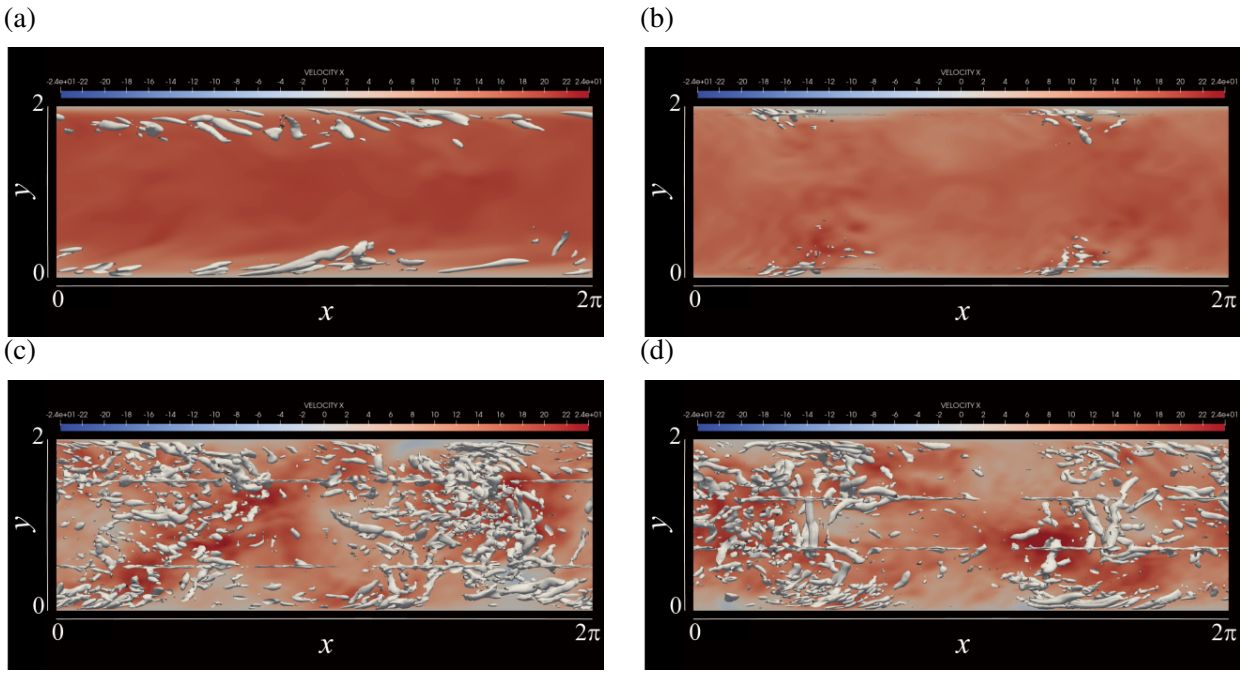

FIG. 6. Instantaneous flow field on the x-y plane: (a) Case NC, (b) Case 1, (c) Case 2, and (d) Case 3. The color contour shows the streamwise velocity at $z = L_z/2$. The white isosurface is the vortical structure visualized by the second invariant of the velocity–deformation tensor. The threshold values of the vortical structures are $Q^+ = 0.03$ and $Q^+ = 0.17$ for Cases NC and 1∼3, respectively.

of vortical structures increases, and turbulence is significantly promoted, indicating a significant increase in skin friction drag and heat transfer.

A three-component decomposition method is introduced to investigate the contribution of the traveling wave to the flow. Previous studies have distinguished contributions based on the direct and indirect effects of traveling waves[5,13]. Accordingly, we define the three-component decomposition method for an arbitrary quantity f as

$$\begin{aligned} f &= \bar{f} + f' \\ &= \langle f \rangle + f'' = \bar{f} + \tilde{f} + f'', \end{aligned} \tag{12}$$

where $\bar{f}$ and $\langle f \rangle$ are defined as

$$\bar{f}(y) = \frac{1}{2\pi} \int_0^{2\pi} \langle f \rangle d\phi_x, \tag{13}$$

$$\langle f \rangle (\phi_x, y) = \frac{1}{N_{\phi_x}} \sum_{x \in \phi_x} \left[\frac{1}{\mathscr{T} L_z} \int_0^{\mathscr{T}} \int_0^{L_z} f(x,y,z,t) dz dt \right], \tag{14}$$

where $\phi_x = \frac{2\pi}{\lambda}(x - ct) - 2\pi n (0 < \phi_x < 2\pi, n \in \mathbb{Z})$ is the wave coordinate along the streamwise direction and $N_{\phi_x} = kL_x/(2\pi)$ is the number of streamwise locations belonging to the same phase. The RSS ($-\overline{u'v'}$) and THF ($-\overline{v'T'}$) are decomposed using the three-component decomposition method as

$$-\overline{u'v'} = -\overline{\tilde{u}\tilde{v}} - \overline{u''v''} \tag{15}$$

$$-\overline{v'T'} = -\overline{\tilde{v}\tilde{T}} - \overline{v''T''}. \tag{16}$$

The LHS is referred to as the "total" component, and the first and second terms on the RHS are referred to as the "coherent" and "random" components.

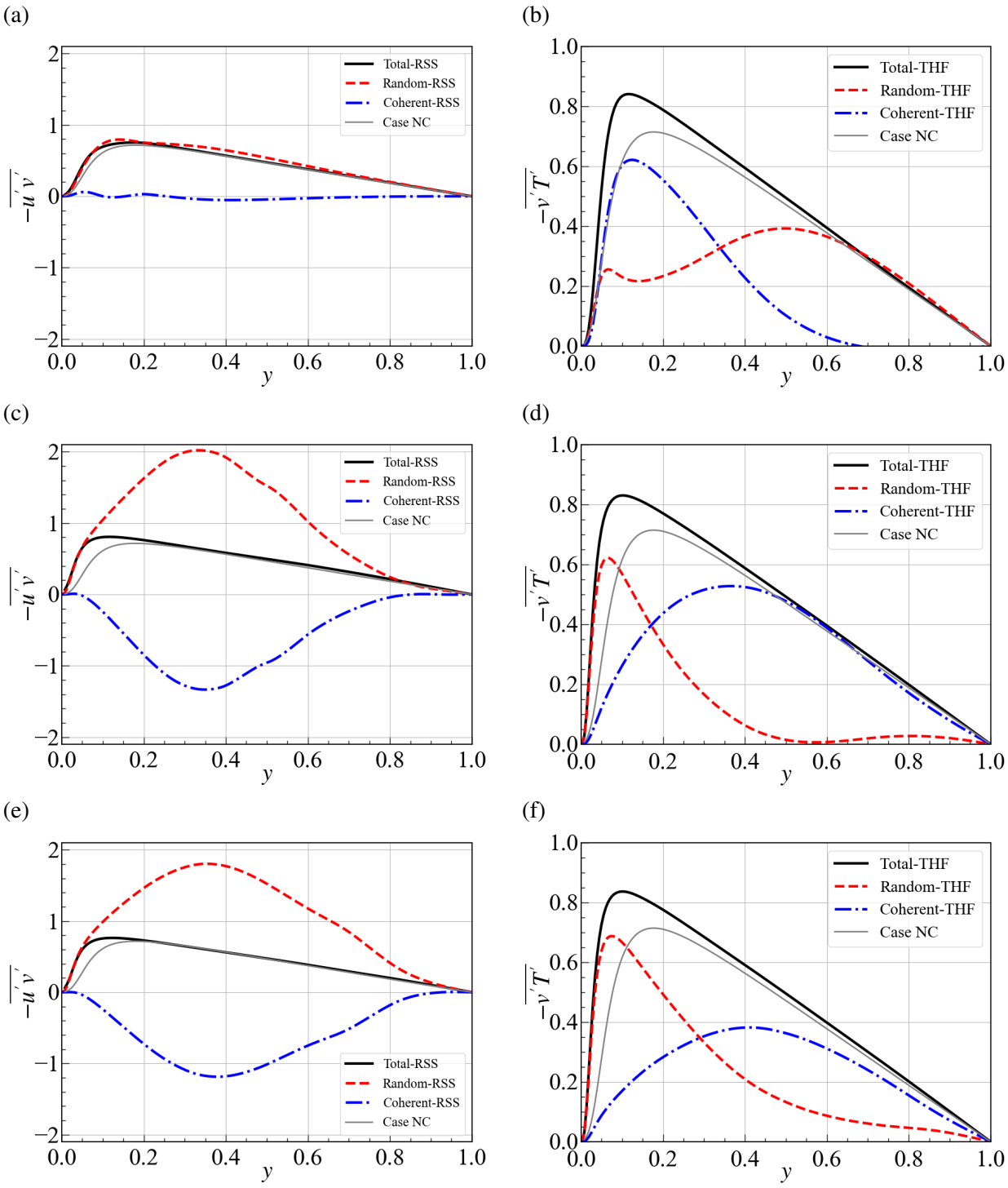

FIG. 7. Decomposed Reynolds share stress (a,c,e) and turbulent heat flux (b,d,f): top, Case 1; center, Case 2; bottom, Case 3. Black, total-RSS; red, random-RSS; blue, coherent-RSS; gray, line, Case NC.

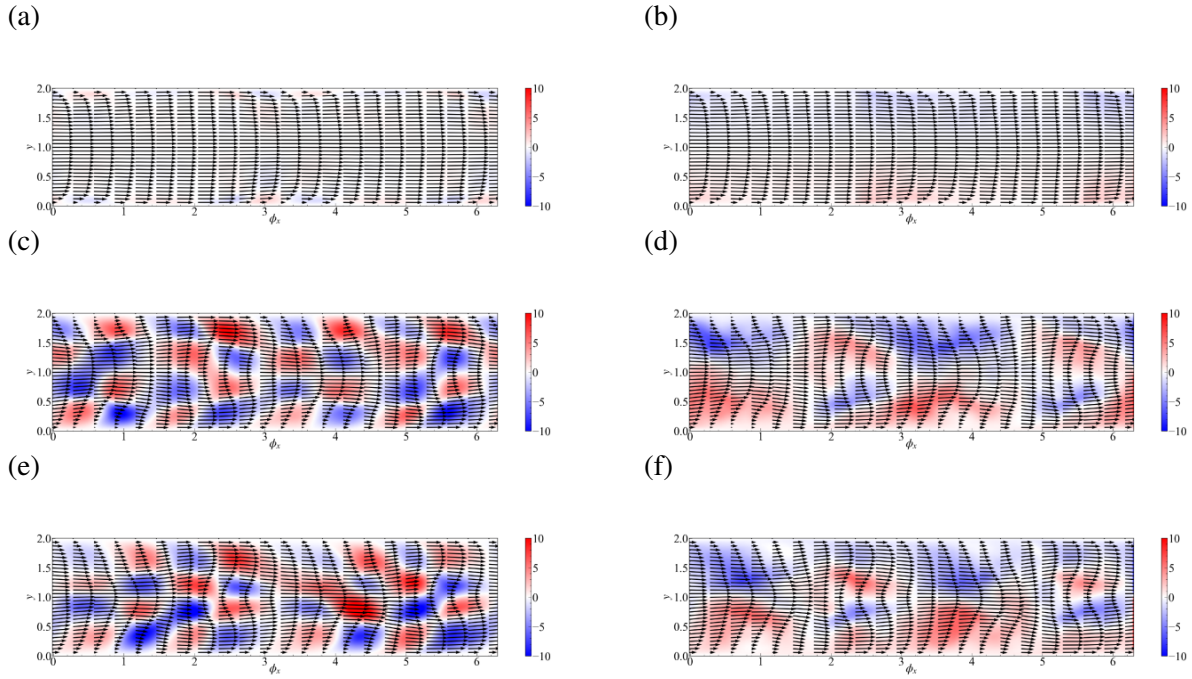

FIG. 8. Distribution of $-\tilde{u}\tilde{v}$ (left) and $-\langle u''v''\rangle$ (rigth): (a,b) Case 1, (c,d) Case 2, and (e,f) Case 3.

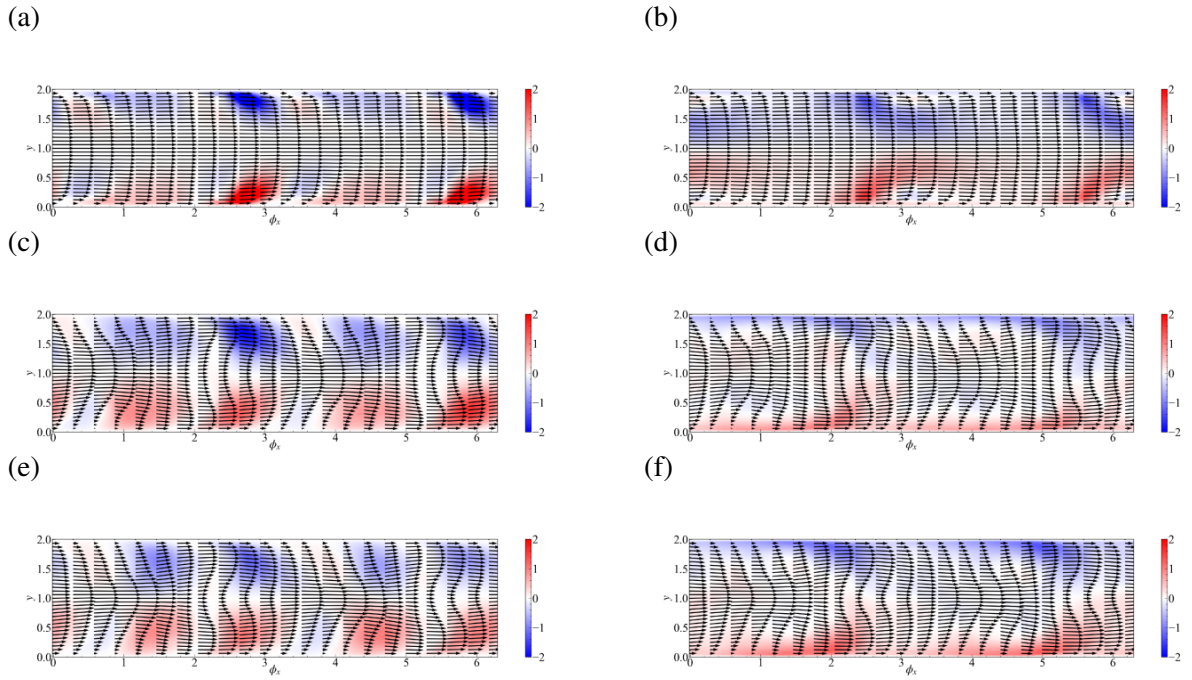

FIG. 9. Distribution of $-\tilde{v}\tilde{T}$ (left) and $-\langle v''T''\rangle$ (right): (a,b) Case 1, (c,d) Case 2, and (e,f) Case 3.

The RSS and THF significantly influenced the skin-friction coefficient and Nusselt number. The decomposed RSS and THF in each case are shown in Fig. 7. The total-RSS in Case 1 is slightly larger than that of Case NC; the random-RSS almost agrees with the total-RSS, and the coherent-RSS is very small. When h_w increases, the coherent-RSS decreases, and the random-RSS increases in Case 2; the peaks slightly decrease and shift toward the channel center in Case 3. Since the traveling wave directly creates the coherent RSS, it moves toward the channel center. The production of the turbulence also creates the random RSS by the wave, it also moves toward the channel center. The random-THF and coherent-THF are positive. The coherent-THF peaks in the region near the wall in Case 1, whereas it attenuates and moves toward the channel center as h_w increases in Cases 2 and 3. However, random-THF had double peaks in Case 1, but the near-wall peak grew, and the other peak decreased and disappeared in Cases 2 and 3.

Figure 8 shows $-\tilde{u}\tilde{v}$ and $-\langle u''v''\rangle$ with the velocity vectors of $\langle u\rangle$ and $\langle u\rangle$. If they are averaged over the wavelength range, they correspond to the RSS and THF. For visibility, the horizontal axis is twice the wavelength. Their distributions were symmetric for the lower and upper halves. In Case 1, the flow deceleration and acceleration were observed in the region near the wall. Although the traveling-wave-like body force from the wall created a spanwise roller-like structure in the region near the wall[5], the roller-like structure is not evident because it is superimposed on the base flow. In addition, $-\tilde{u}\tilde{v}$ and $-\tilde{u}\tilde{v}$ are very small compared with those in Cases 2 and 3. In Case 2, the effect of the wave on the velocity profile is significant; if the near flow is decelerated, the central region is accelerated and *vice versa*. The positive and negative $-\tilde{u}\tilde{v}$ alternate, resulting in the formation of a cellar-like structure. As the negative $-\tilde{u}\tilde{v}$ is superior to the positive one, it results in the positive $\overline{\tilde{u}\tilde{v}}$, as shown in Fig. 7. In contrast, $-\langle u''v''\rangle$ is positive, but a small negative region appears around the center of the channel. A similar distribution is observed in Case 3, whereas the area of $-\langle u''v''\rangle$ around the center region is contracted. The negative $-\langle u''v''\rangle$ decreases (Fig. 8(f)). Figure 9 shows $-\tilde{v}\tilde{T}$ and $-\langle v''T''\rangle$. In Case 1, $-\tilde{v}\tilde{T}$ and $-\tilde{u}\tilde{v}$ are positive and negative in the lower and upper halves, respectively. When h_w increases in Cases 2 and 3, the region of positive and negative $-\tilde{v}\tilde{T}$ expands toward the channel center, whereas $-\tilde{u}\tilde{v}$ distributes in the region near the wall.

Accordingly, the trends exhibited by the coherent-RSS, random-RSS, and coherent-THF are similar, whereas the trend exhibited by random-THF is different. As the random-THF sustains the total-THF for the larger h_w, more significant heat transfer is maintained compared with the skin friction (Fig. 4(b)).

IV. CONCLUSION

The DNS of the turbulent channel flow controlled by a traveling-wave-like wall-normal body force is performed. The control mimicked a self-excited thin film in the corresponding experiment. This study focuses on the effect of the downstream traveling wave on the skin-friction drag, heat transfer, and analogy factor.

The parametric study results demonstrated that the downstream traveling wave enhanced the skin friction and heat transfer. They increased with an increase in h_w, which is the reference location of the traveling wave. The maximum j/f factor was obtained at $h_w = 0.6$. The flow field visualization showed that traveling wave control significantly enhances turbulence, increasing the skin-friction drag and heat transfer. The three-component decomposition method elucidated the variation in the RSS and THF for different values of h_w.

One of the primary mechanisms for the dissimilarity is the opposite signs of the coherent-RSS and -THF. In the case of traveling-wave-like blowing and suction, Higashi *et al.*[22] analyzed the controlled laminar channel flow and revealed that the origin of the dissimilarity is the out-of-phase relationship in the global phase. Kaithakkal *et al.*[13] revealed that the mechanism is the fundamental difference between the divergence-free velocity and passive scalar of the temperature, even in a turbulent flow. In addition, the dissimilarity in the random component was determined by the nonlinear interaction of the coherent field and dissimilarity in the wall-normal gradient of the phase-averaged velocity and temperature field. A similar mechanisms for the dissimilarity between the momentum and heat transfer is assumed and a traveling-wave-like body force away from the wall is employed. When h_w increased, the coherent-RSS, random-RSS, and coherent-RSS moved toward the center; however, the random-THF increased in the near-wall region and decreased away from the wall. Accordingly, it is concluded that the self-excited oscillation of a thin film located in the channel passage induces dissimilarity effects of momentum and heat transfer. Therefore, it is preferable to install a thin film away from the wall.

ACKNOWLEDGMENTS

This study was partially supported by the Ministry of Education, Culture, Sports, Science, and Technology through Grant-in-Aid for Challenging Research (Pioneering) (No. 21K18685) and Grant-in-Aid for Early-Career Scientists (No. 19K14884).

DATA AVAILABITITY

The data that support the findings of this study are available from the corresponding author upon reasonable request.

REFERENCES

[1]K. Fukagata, K. Iwamoto, and N. Kasagi, "Contribution of Reynolds stress distribution to the skin friction in wall-bounded flows," Physics of Fluids **14**, L73–L76 (2002).

[2]N. Kasagi, Y. Hasegawa, K. Fukagata, and K. Iwamoto, "Control of Turbulent Transport: Less Friction and More Heat Transfer," Journal of Heat Transfer **134**, 031009 (2012).

[3]Y. Hasegawa and N. Kasagi, "Dissimilar control of momentum and heat transfer in a fully developed turbulent channel flow," Journal of Fluid Mechanics **683**, 57–93 (2011).

[4]A. Yamamoto, Y. Hasegawa, and N. Kasagi, "Optimal control of dissimilar heat and momentum transfer in a fully developed turbulent channel flow," Journal of Fluid Mechanics **733**, 189–220 (2013).

[5]H. Mamori and K. Fukagata, "Drag reduction effect by a wave-like wall-normal body force in a turbulent channel flow," Physics of Fluids (1994-present) **26**, 115104 (2014).

[6]S. Koganezawa, A. Mitsuishi, T. Shimura, K. Iwamoto, H. Mamori, and A. Murata, "Pathline analysis of traveling wavy blowing and suction control in turbulent pipe flow for drag reduction," International Journal of Heat and Fluid Flow **77**, 388–401 (2019).

[7]Y. Nabae and K. Fukagata, "Bayesian optimization of traveling wave-like wall deformation for friction drag reduction in turbulent channel flow," Journal of Fluid Science and Technology **16**, JFST0024–JFST0024 (2021).

[8]Y. Nabae and K. Fukagata, "Drag reduction effect of streamwise traveling wave-like wall deformation with spanwise displacement variation in turbulent channel flow," Flow, Turbulence and Combustion (2022), 10.1007/s10494-022-00334-w.

[9]K. Uchino, H. Mamori, and K. Fukagata, "Heat transfer in fully developed turbulent channel flow with streamwise traveling wave-like wall deformation," Journal of Thermal Science and Technology **12**, JTST0003–JTST0003 (2017).

[10]R. Nakanishi, H. Mamori, and K. Fukagata, "Relaminarization of turbulent channel flow using traveling wave-like wall deformation," International Journal of Heat and Fluid Flow **35**, 152–159

(2012).

[11]A. M. Akbarzadeh and I. Borazjani, "Large eddy simulations of a turbulent channel flow with a deforming wall undergoing high steepness traveling waves," Physics of Fluids **31**, 125107 (2019).

[12]Y. Nabae, K. Kawai, and K. Fukagata, "Prediction of drag reduction effect by streamwise traveling wave-like wall deformation in turbulent channel flow at practically high Reynolds numbers," International Journal of Heat and Fluid Flow **82**, 108550 (2020).

[13]A. J. Kaithakkal, Y. Kametani, and Y. Hasegawa, "Dissimilarity between turbulent heat and momentum transfer induced by a streamwise travelling wave of wall blowing and suction," Journal of Fluid Mechanics **886**, A29 (2020).

[14]K. Ogino, H. Mamori, N. Fukushima, K. Fukudome, and M. Yamamoto, "Direct numerical simulation of Taylor–Couette turbulent flow controlled by a traveling wave-like blowing and suction," International Journal of Heat and Fluid Flow **80**, 108463 (2019).

[15]H. Mamori, K. Fukudome, K. Ogino, N. Fukushima, and M. Yamamoto, "Heat transfer enhancement and torque reduction by traveling wave-like blowing and suction in turbulent Taylor–Couette flow," Journal of Thermal Science and Technology , in press (2020).

[16]T. Murakami and S. Hara, "Influence of the installation of a rubber sheet on pressure drop and heat transfer characteristics in turbulent channel flow," in *57th annual meeting of the heat transfer society of Japan* (2020) p. B211.

[17]J. Morita, H. Mamori, and T. Miyazaki, "Direct numerical simulation of the backward-facing step turbulent flow controlled by traveling wave-like body force,," International Journal of Heat and Fluid Flow, **95**, 108964 (2021).

[18]K. Fukagata, N. Kasagi, and P. Koumoutsakos, "A theoretical prediction of friction drag reduction in turbulent flow by superhydrophobic surfaces," Physics of Fluids **18**, 051703 (2006).

[19]K. Fukagata and N. Kasagi, "Highly Energy-Conservative Finite Difference Method for the Cylindrical Coordinate System," Journal of Computational Physics **181**, 478–498 (2002).

[20]J. Kim, P. Moin, and R. Moser, "Turbulence statistics in fully developed channel flow at low Reynolds number," Jouornal of Fluid Mechanics **177**, 133–166 (1987).

[21]H. Kawamura, H. Abe, and K. Shingai, "Dns of turbulence and heat transport in a channel flow with different reynolds and prandtl numbers and boundary conditions," in *Turbulence, Heat and Mass Transfer 3 (Proc. of the 3rd International Symposium on Turbulence, Heat and Mass Transfer)* (2000) pp. 15–32.

[22]K. Higashi, H. Mamori, and K. Fukagata, "Simultaneous Control Of Friction Drag Reduction And Heat Transfer Augmentation By Traveling Wave-Like Blowing/Suction," Computational Thermal Sciences: An International Journal **3**, 521–530 (2012).